



1    **Role of hydrometeorological variables and catchment area to flood generation over**  
2    **the monsoonal climate region of India**

3    **Authors**

4    Saran Aadhar<sup>1,2</sup>, Efrat Morin<sup>3</sup>, Utkarsh Gupta<sup>1</sup>

5    **Affiliations**

- 6        1. Civil and Infrastructure Engineering, Indian Institute of Technology (IIT)  
7                Jodhpur, Jodhpur, India
- 8        2. Center for Emerging Technologies for Sustainable Development (CETSD), IIT  
9                Jodhpur, Jodhpur, India
- 10      3. The Fredy & Nadine Herrmann Institute of Earth Sciences, Hebrew University of  
11                Jerusalem, Jerusalem, Israel

12    **Corresponding Author:** Saran Aadhar (saran.aadhar@iitj.ac.in)

13

14    **Abstract:**

15    Indian River basins experience frequent flooding during the Indian summer monsoon  
16    rainfall and pose several challenges to the large population of the region. To effectively  
17    manage flood risk in the region, a better understanding of flood-generating mechanisms  
18    is essential, yet hydrometeorological and catchment drivers controlling flood processes  
19    are poorly explored across India. In this study, we examine the role of  
20    hydrometeorological variables (such as precipitation and surface runoff) and catchment  
21    area in the flood occurrence in one of the largest river basins (Godavari River basin) of



22 the Indian Subcontinent using observed and VIC-simulated datasets. Based on the  
23 temporal analysis of precipitation, runoff, and streamflow, we show that floods caused by  
24 multiple high-intensity precipitation days predominantly occur in the semi-humid sub-  
25 basins (Tekra, Pathagudam, Perur, and Polavaram) of the Godavari River. The majority  
26 of floods in the semi-humid sub-basins are associated with 10 to 11 days of accumulated  
27 precipitation, having multiple high-intensity precipitation events prior to flood. In  
28 contrast, the majority of floods in the semi-arid region of Godavari (Mancherial sub-  
29 basin) are triggered by a single high-intensity precipitation day and associated with short-  
30 duration (2 days) accumulated precipitation. In addition to temporal analysis, we also  
31 performed Empirical Orthogonal Functions (EOF) analysis using precipitation, runoff,  
32 and streamflow data to identify the flood-dominant catchment area. Our results  
33 demonstrate that central and downstream areas of the basin contribute disproportionately  
34 to flood occurrence, with the Tekra sub-basin generating substantially higher runoff due  
35 to favorable catchment characteristics. Overall, this study advances understanding of  
36 flood-generating mechanisms over the Godavari River basin, which can be helpful for  
37 flood control and management during the monsoonal climate of the Indian Subcontinent.

38 **Keywords:** Flood mechanisms, Hydrometeorology, Catchment Characteristics, Godavari  
39 basin, Monsoonal climate.

40 **Highlights**

41 • The majority of floods in the semi-humid regions of the Godavari River  
42 predominantly occur due to multiple high-intensity rainfall days  
43 • Floods in the semi-arid Mancherial sub-basin are triggered by a single high-  
44 intensity precipitation event



45        • **Central and downstream areas of the Godavari River basin dominate in the**  
46        **flood occurrence**  
47        • **High runoff generation in the Tekra sub-basin plays an important role in**  
48        **downstream flooding in the Godavari River basin**

49

50        **1. Introduction**

51        Floods are one of the costliest natural disasters, which cause severe damage to  
52        infrastructure and socio-economic conditions. According to the World Bank report in 2006,  
53        floods caused damage of 163 million US\$ annually during the 1999–2005 period in India.  
54        Moreover, the occurrence of floods has increased in India in the last few decades under the  
55        warming climate, which has affected millions of people in the region (Ali et al., 2019;  
56        Gosain et al., 2006; Gupta and Nair, 2011; Milly et al., 2002). For instance, recently  
57        occurred flood events in the Indian sub-continent (i.e., 2018 Kerala flood, 2014 Jammu and  
58        Kashmir flood, 2013 Uttarakhand flood) caused enormous loss of property and human lives  
59        (Lindell et al., 2019; Mishra et al., 2018; Ray et al., 2019). Due to global warming, the  
60        frequency of high-intensity precipitation events has increased at the regional and global  
61        scales (Allan and Soden, 2007; Gosain et al., 2006; Guerreiro et al., 2018; Min et al., 2011;  
62        Rogger et al., 2017; Trenberth et al., 2003; Ummenhofer et al., 2011), which instigated the  
63        increase in flood magnitude and frequency across the globe (Ali et al., 2019; Gosain et al.,  
64        2006; Gupta and Nair, 2011; Kundzewicz et al., 2014; Milly et al., 2002). Therefore, an  
65        improved understanding of flood processes is required in the densely populated Indian sub-  
66        continent to reduce the severe impact of flood events.



67        Flood mechanisms comprise multiple processes that control the intensity and  
68        magnitude of flow in a river. In the monsoonal climate, the majority of floods occur  
69        primarily due to high-intensity precipitation events (Ali et al., 2019; Garg and Mishra,  
70        2019; Nanditha et al., 2022; Nanditha and Mishra, 2022). However, static factors of  
71        catchment properties (basin slope, geometry, land use land cover, drainage density,  
72        drainage area, and soil parameters) can also have an essential role in the flood generation  
73        mechanism, apart from extreme precipitation (Blöschl et al., 2017, 2013; Merz and Blöschl,  
74        2003; Tarasova et al., 2019). For example, forest land cover generates less runoff than  
75        arable land cover during storm events (Lane, 2017; Marc and Robinson, 2007).

76        To examine flood control processes, several causative processes and storylines  
77        (e.g., high precipitation, rain on snow, cloudburst, excess runoff) have been used in  
78        previous studies (Berghuijs et al., 2016; Keller et al., 2018; Li et al., 2019; Nied et al.,  
79        2014; Tarasova et al., 2019; Viglione et al., 2010). These causative processes include the  
80        hydroclimatic, hydrological, and hydrograph perspectives to better understand the flooding  
81        mechanisms (Tarasova et al., 2019). Based on the causative classification, the flood  
82        mechanisms, considering the weather systems, storm patterns, moisture transport, and  
83        weather circulation, are classified in the hydroclimatic perspective (Blöschl et al., 2013;  
84        Grams et al., 2014). Hydrograph perspective uses discharge time-series data to evaluate the  
85        different hydrographs, which show distinct flood generation mechanisms (Tarasova et al.,  
86        2019). Under the hydrological perspective, hydrometeorological variables within the  
87        catchment, soil moisture information, and hydrological processes (i.e., saturation excess  
88        and infiltration) are considered (Berghuijs et al., 2016; Nied et al., 2014; Sikorska et al.,  
89        2015).



90        In some cases, multiple criteria were used in the evaluation of flood processes, for  
91        example, short-duration heavy rainfall and long-duration rainfall (with and without high-  
92        intensity rainfall) (Keller et al., 2018; Li et al., 2019; Nied et al., 2014; Tarasova et al.,  
93        2019). Additionally, the spatial variability of hydrometeorological variables within the  
94        catchment is also crucial to the flooding mechanism. For instance, Freyberg et al. (2014)  
95        found that a small portion of the catchment induces large streamflow in a pre-alpine  
96        catchment during the rainy days, which causes floods in the basin. Therefore, determining  
97        the flood-dominating catchment areas based on the hydrometeorological and catchment  
98        properties before the peak flood is crucial for understanding flood processes. Overall, we  
99        need to thoroughly analyze the temporal and spatial properties of hydrometeorological  
100        variables for a better understanding of flood generation mechanisms.

101        Flood mechanisms remain largely unexplored in large rivers within the monsoonal  
102        climate of India, which presents unique conditions of hydrometeorology and catchment  
103        properties. For instance, large river basins of India have dry soil conditions in the pre-  
104        monsoon season, while extremely wet soil conditions during the mid and late monsoon.  
105        Moreover, large basins exhibit a variety of climate zones, topographies, soil parameters,  
106        and vegetation covers, which result in different hydrological responses during the monsoon  
107        season. Therefore, the goal of the present study is to understand the major flood-generating  
108        mechanisms in one of the largest river basins in the Indian Subcontinent, the Godavari  
109        River basin. Using the Variable Infiltration Capacity [VIC; (Cherkauer et al., 2003; Liang  
110        et al., 1996, 1994)] simulated hydrological variables and observed meteorological datasets,  
111        first, we examine the temporal variability of hydrometeorological variables (precipitation  
112        and surface runoff) before the peak streamflow events to identify the dominating flood



113 processes. Later, we evaluate the spatial variability of hydrometeorological variables to  
114 identify flood-dominant catchment areas, which are associated with the occurrence of  
115 downstream flood events.

116 **2. Study area**

117 The Godavari River basin (Figure 1) is the second largest river basin in India, after  
118 the Ganges basin. The Godavari River witnessed many severe floods in the past decades  
119 (Garg and Mishra, 2019; Mujumdar et al., 1969; Rakhecha and Singh, 2017; Rakhecha,  
120 2002), which affected the livelihood and life of millions of people in the basin. For instance,  
121 the floods during the year 1969 and 1976 in the Indravati (tributary of the Godavari River)  
122 stream posed severe damage in the basin (Garg and Mishra, 2019; Mujumdar et al., 1969;  
123 Rakhecha, 2002), which resulted in enormous loss of property and human lives. Similarly,  
124 the year 1986 flood in the downstream part of the river affected millions of people, with a  
125 loss of more than 250 lives (Rakhecha and Singh, 2017; The Hindu, 2011). Moreover, the  
126 high flow level in the Godavari River during 2019 displaced more than 17000 people of  
127 Andhra Pradesh (<https://floodlist.com/asia/india-godavari-river-flood-andhra-pradesh-august-2019>).

129 The Godavari river basin has a drainage area of approximately 312,800 km<sup>2</sup> and a  
130 river length of 1,465 km. The basin covers six Indian states (Maharashtra, Karnataka,  
131 Andhra Pradesh, Telangana, Chhattisgarh, and Odisha) and is located in peninsular India.  
132 Godavari River originates from Triambakeshwar, a high-altitude (1067 m above sea level,  
133 masl) place in the Nasik district of Maharashtra. The river flows eastward from the Western  
134 Ghats to the Bay of Bengal across the Deccan Plateau (Figure 1). The basin exhibits  
135 significant elevation variability (Figure 1a), ranging from a flat plain (below 10 masl) to a



136 hill range (above 1200 masl). Due to its low elevation, the downstream part of the basin  
137 has experienced numerous floods in the past. For instance, the irrigation department of  
138 Andhra Pradesh issued 22 flood warnings between 1962 and 1990 at Dowlaismwarm (the  
139 place is located near the river mouth) (Nageswara Rao, 2001). The basin also shows a large  
140 diversification in land use and land cover (LULC). The upper part of the basin is primarily  
141 covered by irrigated agricultural land, while the downstream region has forest land cover  
142 (Figure 1b).

143 There is a large spatial variation in climate conditions across the basin. The annual  
144 mean temperature of the basin varies between 20 to 30 °C, primarily correlated with  
145 elevation (Figure 1c). Moreover, the Godavari river basin receives the majority of  
146 precipitation in the form of rainfall (without any snowfall), which predominantly occurs  
147 during the monsoon season (June to September), with large spatial variability in the annual  
148 mean (Figure 1d). The annual mean precipitation varies from 500 to 1200 mm, where the  
149 eastern part of the basin receives a large amount of rainfall, while the western part receives  
150 less than 600 mm of precipitation during the monsoon season (Figure 1d). Based on the  
151 Aridity Index (AI; the ratio of mean annual precipitation and mean annual potential  
152 evapotranspiration), the western part of the Godavari basin falls under the semi-arid region  
153 ( $0.2 \leq AI < 0.5$ ) due to less rainfall (Figure S1), while the central and eastern parts of the  
154 basin fall under dry semi-humid and wet semi-humid region, respectively (Figure S1).  
155 Detailed information about the basin elevation, land use land cover (LULC), precipitation,  
156 and temperature can be obtained from Figure 1.

157 We selected five streamflow stations (Mancherial, Tekra, Pathagudam, Perur, and  
158 Polavaram; Figure 1a) for our analysis, which are located at major river reaches of the



159 Godavari River. The Mancherial, Tekra, and Pathagudam stations are on reaches that drain  
160 into the reach measured by the Perur station, which in turn, drains into the Polavaram  
161 station. Based on the area of catchment, Pathagudam is the smallest sub-basin with around  
162 35,625 km<sup>2</sup> area, followed by Mancherial (84,375 km<sup>2</sup>), Tekra (90,625 km<sup>2</sup>), and Perur  
163 (226,250 km<sup>2</sup>) sub-basins. Polavaram is the largest sub-basin, covering approximately  
164 257,500 km<sup>2</sup>.

165

166 **3. Data and methods**

167 **3.1. Observed data**

168 We used the daily meteorological forcing for hydrological modeling to simulate the  
169 streamflow from 1967-2019 over the Godavari River basin. Daily precipitation, minimum  
170 and maximum temperature, and wind speed datasets were used to develop the daily  
171 meteorological forcing. We obtained daily 0.25° gridded observed precipitation data from  
172 the India Meteorological Department [IMD, (Pai et al., 2014)]. IMD developed daily  
173 gridded precipitation data at 0.25° spatial resolution using the approximately 6995 stations  
174 located across the country using the inverse distance weighted interpolation scheme (Pai et  
175 al., 2015). Daily maximum and minimum temperature data were also obtained from the  
176 IMD at 1° spatial resolution based on 395 stations located across India (Srivastava et al.,  
177 2009). To maintain consistency in spatial resolution, maximum and minimum temperature  
178 data were regridded at 0.25° using a lapse rate relationship and digital elevation model  
179 (DEM) described by Maurer et al. (2002). The precipitation and temperature data from  
180 IMD capture the spatial and temporal variability well across India and have been used  
181 widely in previous studies (Chawla and Mujumdar, 2015; Garg and Mishra, 2019; Mahto



182 and Mishra, 2019; Rajeevan et al., 2012; Shah and Mishra, 2016). The gridded wind data  
183 is not available from IMD. Therefore, we collected reanalysis wind speed data from the  
184 National Centers for Environmental Prediction- National Center for Atmospheric Research  
185 (NCEP-NCAR), which is available at 0.25° spatial resolution. Daily streamflow discharge  
186 data for model calibration and validation were obtained from the Central Water  
187 Commission (CWC) for the five selected gauging stations (Mancherial, Tekra,  
188 Pathagudam, Perur, and Polavaram), for the period 1967-2014. Streamflow data after 2014  
189 have too many gaps and therefore could not be used for our analysis.

190 **3.2. The Variable Infiltration Capacity (VIC) and routing models**

191 The VIC model (Cherkauer et al., 2003; Cherkauer and Lettenmaier, 1999; Liang  
192 et al., 1996, 1994) is a physically based, land surface, grid-based hydrologic model that  
193 simulates energy and water fluxes at daily and sub-daily timescales for each grid cell (Gao  
194 et al., 2010). The hydrological model considers the soil parameters, vegetation parameters,  
195 including their sub-grid variability, and meteorological forcing (precipitation, maximum  
196 and minimum temperature, and wind speed data) to simulate surface runoff, baseflow,  
197 evaporation, and soil moisture. The sub-grid variability of soil and vegetation makes the  
198 VIC model more realistic than other physically-based models in heterogeneous  
199 topographic regions (Gao et al., 2012). Vegetation parameters for the VIC model were  
200 extracted from the Advanced Very High-Resolution Radiometer (AVHRR) global land-  
201 cover information, which is available at 1km spatial resolution (Hansen et al., 2000;  
202 Sheffield and Wood, 2007). We used the Harmonized World Soil Database [HWSD;  
203 (Fischer et al., 2008)] soil data to develop soil parameters for the VIC model. For the given  
204 parameters and meteorological data, the VIC model uses the Xinanjiang model (Ren-Jun,



205 1992) and Richard's equation (Liang et al., 1994) to estimate the runoff and soil moisture,  
206 respectively. VIC considers three layers of soil. Out of the three, only the top two soil layers  
207 contribute to the estimation of surface runoff, while the bottom layer contributes to  
208 baseflow estimation.

209 Along with the VIC model, the stand-alone routing model from Lohmann et al.,  
210 (1996) was used to route surface runoff and baseflow simulated by the VIC to desired  
211 locations over the basin. The model is based on two parts, routing within grid cell and  
212 channel routing, where the first uses the unit hydrograph method while the second is  
213 performed using the linearized Saint-Venant equation. Both parts of the routing model are  
214 developed using the simple linear transfer function (Gao et al., 2010). The streamflow  
215 routing model assumes that surface runoff and baseflow exit a cell in a single flow direction  
216 based on the topography. Basin and sub-basin delineation and flow direction were  
217 computed from the Shuttle Radar Topography Mission elevation data (Digital Object  
218 Identifier (DOI) number: /10.5066/F7PR7TFT) for the routing model.

219 We used the previously calibrated VIC model of the Godavari River basin from  
220 Garg and Mishra (2019). Garg and Mishra (2019) calibrated the VIC model using the six  
221 soil parameters:  $Ds_{max}$  (maximum velocity of baseflow),  $Ds$  (Fraction of  $Ds_{max}$  where  
222 nonlinear baseflow begins),  $W_s$  (fraction of the maximum soil moisture where nonlinear  
223 baseflow occurs),  $b_{inf}$  (shape of the variable infiltration capacity curve), and soil depths of  
224 the second and third layers; which control surface runoff, baseflow, evaporation (in bare  
225 soil), and soil moisture in the VIC model. The infiltration shape parameter ( $b_{inf}$ ) and soil  
226 depths are used in the estimation of surface runoff, infiltration, soil moisture, and bare soil  
227 evaporation, while  $Ds_{max}$ ,  $Ds$ , and  $W_s$  parameters are mainly used for baseflow estimation.



228 More information on the VIC model, input datasets, and parameters can be obtained from  
229 Gao et al., (2010) and the Land Surface Hydrology Research Group at the University of  
230 Washington (<http://uw-hydro.github.io/>).

231 In this study, the calibrated VIC model (Garg and Mishra, 2019) was re-evaluated  
232 for the five stations using the updated observed daily streamflow data (Figure S2, Table  
233 S1, S2). We re-evaluated the model performance for the Mancherial, Tekra, Pathagudam,  
234 Perur, and Polavaram stations of the Godavari River basins for the 1970-2014 period,  
235 where the first 10 years are the calibration period (Garg and Mishra, 2019) and the rest is  
236 the validation period (Figure S2, Table S1). The model performance was evaluated using  
237 the Nash–Sutcliffe efficiency [NSE; (Nash and Sutcliffe, 1970)], the coefficient of  
238 determination ( $R^2$ ), and bias percentage at low (Bias\_Q5), mean (Bias\_mean), and high  
239 (Bias\_Q95) streamflow values. These metrics (NSE,  $R^2$ , and Bias values) show that the VIC  
240 model performs satisfactorily during the calibration period (Table S1, Figure S2) and has  
241 an acceptable performance during the validation period (Table S2, Figure S2).

242 In the present study, we did not consider the interventions of human activities in  
243 the water cycle due to the limited availability of human intervention datasets. However,  
244 human activities in the basin do not affect the natural river flow in the majority of sub-  
245 basins except for the semi-arid region of the Mancherial sub-basin. A large number of  
246 reservoirs were constructed for water storage in this region, which affected the model  
247 performance, mostly after 1994. Therefore, the validation period was limited to 1980-1993  
248 for the Mancherial station (Figure S2, Table S2). Such effects were not found in the  
249 downstream stations of Perur and Polavaram since the streamflow volume contribution of  
250 the semi-arid Mancherial basin is low relative to the rest of the basin area of these two



251 basins. Overall, our results showed that the VIC simulated natural streamflow compares  
252 well against the observed daily streamflow for all five stations during the calibration and  
253 validation period (Figure S2, Table S1, S2). Therefore, the use of VIC (without human  
254 intervention) simulated streamflow is acceptable for our analysis.

255

### 256 **3.3. Flood event characterization**

257 To understand the flood generation mechanism, we evaluated two major aspects over  
258 the Godavari river basin (Figure 2): (i) temporal properties of flood-causing precipitation  
259 and surface runoff, and (ii) flood-dominating catchment area.

260 These analyses were based on observed precipitation data and VIC-simulated runoff  
261 and streamflow data. As the focus here is on floods, we identified independent high-  
262 streamflow events using the peak-over-threshold approach. First, we selected the daily  
263 streamflow discharge more than the 95<sup>th</sup> percentile threshold value to determine the high-  
264 streamflow events. Later, we grouped the events that occurred with less than 10 days of  
265 separation (Brunner et al., 2020a, 2020b; Diederens et al., 2019) to identify the independent  
266 high-streamflow event. If two or more high-streamflow events occurred together within  
267 each separation (within 10 days), we used the highest discharge value to make the event  
268 independent.

#### 269 **3.3.1. Temporal properties of flood-causing precipitation and surface runoff**

270 Based on the duration of precipitation that leads to flood events, the events can be  
271 classified into long or short rain flood types (Berghuijs et al., 2016; Merz and Blöschl,  
272 2003). Accordingly, we performed a temporal analysis of precipitation and runoff to



273 identify the flood types. The correlation between the event peak discharge and basin area-  
274 averaged accumulated precipitation (before the peak streamflow) for different durations  
275 (range of 1-20 days) and lag times (0-7 days, representing the lag between the end of the  
276 precipitation window and the day of the peak streamflow) was estimated for all five sub-  
277 basins. A similar analysis was conducted by correlating the event peak discharge with  
278 accumulated surface runoff prior to the peak.

279 The precipitation in the time windows found most correlated with the peak discharge was  
280 further analyzed to identify three flood-generation storylines, following the studies by  
281 Keller et al., (2017) and Berghuijs et al., (2016): (i) flood caused by a single high-intensity  
282 precipitation day; (ii) flood caused by multiple high-intensity precipitation days; and (iii)  
283 floods caused by low-to-medium intensity precipitation days. For this, we checked the  
284 number of high precipitation days (above 99<sup>th</sup> percentile) within the relevant window prior  
285 to the flood event. If the number is one, it is identified as caused by a single high  
286 precipitation day. If it is more than one, then the flood event is caused by multiple high-  
287 intensity precipitation days. Finally, if both conditions fail and there is no high precipitation  
288 day prior to the flood, then the flood event is caused by multiple low-to-medium intensity  
289 precipitation days.

290 **3.3.2. Flood-dominating catchment area**

291 Next, we evaluated the dominated catchment area in flood generation by examining the  
292 precipitation and runoff spatial variability (Figure 2). For that, we used the empirical  
293 orthogonal function (EOF) analysis and obtained the leading modes of spatial variability  
294 in precipitation and surface runoff (Mishra et al., 2012). In the EOF analysis, we used the  
295 accumulated precipitation and surface runoff at each pixel for the time windows found



296 most correlated with peak discharge, according to the findings in step 1 above. Lastly, we  
297 examine the role of antecedent soil moisture conditions in the runoff generation  
298 mechanism. We categorize all flood events into dry and wet conditions based on the soil  
299 moisture simulated for the first soil layer before the time window found most correlated  
300 with peak discharge. If the soil moisture is more than 75<sup>th</sup> percentile, the flood event is  
301 identified as a wet condition or vice versa. Thereafter, we analyzed the mean runoff  
302 coefficient (surface runoff divided by precipitation) for wet and dry conditions for the time  
303 window found in step 1.

304

305 **4. Results**

306 **4.1. High-intensity precipitation and Discharge Flood events**

307 Using the daily precipitation and simulated discharge data, we estimated the high-  
308 intensity precipitation and streamflow values (precipitation and discharge values above  
309 95<sup>th</sup> percentile;  $P_{95}$  and  $Q_{95}$ ) for each month at the Mancherial, Tekra, Pathagudam, Perur,  
310 and Polavaram stations, considering the 95<sup>th</sup> percentile threshold value of the period  
311 1967-2019 (Figure S3). The majority of high-intensity precipitation ( $P_{95}$ ) and streamflow  
312 ( $Q_{95}$ ) occurred during the monsoon months (June-September; Figure S3a-e). The ratio of  
313 high-intensity streamflow and precipitation values varies with time. The early months of  
314 monsoon (i.e., June and July) have a low ratio of  $Q_{95}$  and  $P_{95}$  compared to late monsoon  
315 months (i.e., August and September). Due to dry initial soil moisture conditions, the  
316 majority of high-intensity precipitation that occurred in June and July did not cause high  
317 streamflow in the Godavari River. However, most high-intensity precipitation events



318 cause high streamflow in August and September due to wet soil moisture conditions in  
319 the late monsoon season (Figure S3). Moreover, we noticed a higher ratio of  $Q_{95}$  and  $P_{95}$   
320 in October in the Mancherial sub-basin, which is associated with wet moisture conditions  
321 and the onset of the Northeast monsoon in the sub-basin (Mishra et al., 2021; Rajeevan et  
322 al., 2012a). Our preliminary analysis indicates the significant role of high-intensity  
323 precipitation and antecedent soil moisture conditions in the high-intensity streamflow  
324 occurrence over the Godavari basin, which is consistent with the previous study of Garg  
325 and Mishra (2019).

326 To further understand the role of high-intensity precipitation and runoff in basin floods,  
327 first, we identified flood events (independent high streamflow events as described in the  
328 method section) for each sub-basin during the period 1967-2019 (Figure 3a). We found a  
329 total of 116, 107, 88, 105, and 104 independent high streamflow events in the  
330 Mancherial, Tekra, Pathagudam, Perur, and Polavaram stations, respectively, during the  
331 period 1967-2019 (Figure 3a). Using the identified flood events, we analyzed the  
332 temporal and spatial variability of precipitation and runoff in further analysis to  
333 understand the attribution of hydrometeorological variables and catchment area to flood  
334 generation.

335 **4.2. Temporal properties of flood-causing precipitation and surface runoff**

336 Next, we analyzed the temporal properties of precipitation before the peak  
337 streamflow of flood events. We found (Table 1, Table S3-S7) that the highest correlation  
338 between the basin-averaged accumulated precipitation and the peak streamflow is for lags  
339 of 1-2 days and durations that vary between stations. Floods in the semi-arid Mancherial  
340 sub-basins were linked with short-duration (2 days) precipitation events (Table S3) while



341 floods at other sub-basins (Tekra, Pathagudam, Perur, and Polavaram, Tables S4-S7)  
342 were correlated well with long-duration (10-11 days) precipitation. Similarly, we  
343 analyzed the temporal dynamics of surface runoff before the occurrence of peak  
344 streamflow (Table 2, Tables S8-S12). As expected, the Mancherial sub-basin showed the  
345 highest correlation with short-duration (2 days) accumulated runoff, while for the other  
346 sub-basins, the highest correlation was found with long-duration (7-8 days) accumulated  
347 runoff (Table 2). The temporal properties of surface runoff are similar to precipitation but  
348 with a smaller time window, which is due to the depletion of some of the precipitation  
349 into soil storage. Overall, we found that the floods in large parts of the Godavari basin are  
350 associated with long-duration precipitation and surface runoff except for the Mancherial  
351 sub-basin, where the floods are characterized by short-duration precipitation and surface  
352 runoff (Tables 1, 2).

353 The precipitation in the time window presented above was further analyzed for  
354 the three different conditions (see Section 3.3.1). We found that for four out of five sub-  
355 basins (Tekra, Pathagudam, Perur, and Polavaram), the majority of flood events (around  
356 40-50%) occurred due to multiple high-intensity precipitation (more than 99<sup>th</sup> percentile)  
357 days (Figure 3b). However, most of the floods in the Mancherial sub-basin occurred due  
358 to single high-intensity precipitation days (Figure 3b). This is not surprising, given the  
359 shorter precipitation duration found for Mancherial compared to the other sub-basins. We  
360 also found that around 30-40% flood events in Mancherial, Perur, and Polavaram sub-  
361 basins are associated with long-term low-intensity precipitation (Figure 3b). Overall, our  
362 results showed that the majority of flood events in Tekra, Pathagudam, Perur, and  
363 Polavaram sub-basins occurred due to the higher attribution of multiple high-intensity



364 precipitation days. However, the majority of flood events in the Mancherial sub-basin  
365 occurred due to higher attribution of single-day high-intensity precipitation (Figure 3,  
366 Table 1, 2).

367 **4.3. Flood-dominating catchment area**

368 Next, we identify the catchment area, which dominantly contributes to the flood  
369 generation mechanism. The flood-dominating catchment area is identified based on the  
370 spatial variability of hydrometeorological variables (precipitation and surface runoff  
371 patterns) and catchment conditions before the peak streamflow. Using the EOF analysis,  
372 we estimated the leading spatial patterns of variability in the accumulated precipitation  
373 and surface runoff before the peak streamflow, where accumulation of precipitation and  
374 runoff was based on the time-windows estimated in the previous analysis (i.e., 2, 10, and  
375 11 days for precipitation and 2, 7, and 8 days for runoff, Tables 1, 2).

376 Based on EOF analysis, we found that flood-causing precipitation occurred  
377 predominantly in downstream areas of the Mancherial and Tekra sub-basins, which reside  
378 in the central part of the Godavari basin (Figure 4a-c). However, the leading spatial  
379 pattern (Mode-1) of accumulated precipitation covers the entire region of Pathagudam  
380 (Figure 4a-c). Perur sub-basin also showed a similar spatial pattern of EOF analysis for  
381 the 10 and 11 days accumulated precipitation and indicated the high weightage over the  
382 central and downstream parts of the sub-basins during flood generation (Figure 4e-h). For  
383 the Polavaram sub-basin, we found a high dominance of the central and downstream part  
384 of the Godavari basin in the flooding mechanism (Figure 4i-k). Moreover, the correlation  
385 between peak streamflow and the leading mode (mode-1) of 10 or 11 days of  
386 accumulated precipitation is higher than the leading mode of 2 days of accumulated



387 precipitation (Figure 4d) due to long-rain type floods at Tekra, Pathagudam, Perur, and  
388 Polavaram sub-basins (Table 1). Furthermore, EOF analysis for accumulated surface  
389 runoff (Figure 5) showed a similar leading spatial pattern, although its area is slightly  
390 smaller compared to the precipitation (Figure 4). Other than EOF analysis, we also  
391 computed the pixel-based correlation between accumulated precipitation and peak  
392 streamflow (Figure S4) and between accumulated runoff and peak streamflow (Figure  
393 S5), for each sub-basin over the relevant duration. Our results showed spatial patterns of  
394 correlation analysis that were similar to those obtained from the EOF analysis. In  
395 addition, our analysis (Figure S4 and Figure S5) confirms the previous finding (Figure 4  
396 and Figure 5) where higher correlations of peak streamflow in the Tekra, Pathagudam,  
397 Perur, and Polavaram sub-basins are with long-duration precipitation and runoff,  
398 compared to short-duration, while for the Mancherial station, the opposite behavior was  
399 found.

400 We further estimated the pixel-based runoff coefficient (ratio of surface runoff to  
401 precipitation) before the peak streamflow for 2, 7, and 8 days durations under both dry  
402 and wet soil moisture conditions (Figure 6). We found that the Tekra basin showed the  
403 highest values of runoff coefficient compared to the other parts of the basin for all  
404 durations and in both wet and dry conditions (Figure 6), indicating the dominance of the  
405 Tekra sub-basin in the Godavari river flooding. We also found that the variation in runoff  
406 coefficient among durations is lower during the dry conditions compared to the wet  
407 conditions (Figure 6). For instance, under wet conditions, the values of the runoff  
408 coefficient are higher for the 2 days duration and decrease slightly for 7 and 8-day  
409 durations. The decrease in runoff coefficient for 7 and 8 days durations is due to the



410 lower intensity of rainfall in long-time span compared to 2 days duration rainfall.  
411 However, we found that runoff coefficient values are quite similar for all durations under  
412 the dry condition. Overall, our results highlight the flood-dominated area of the Godavari  
413 basin based on the hydrometeorology and catchment properties. Our analysis reveals that  
414 the central region of the Godavari basin and the Tekra sub-basin contribute significantly  
415 to flood generation, compared to other parts of the basin. Furthermore, these results can  
416 be used for flood management in the basin.

417

## 418 **5. Discussion and Conclusions**

419 Floods pose severe challenges to the infrastructure, ecology, and socio-economic  
420 development of the largely populated Indian Subcontinent. Moreover, the risk of floods  
421 has increased significantly under global warming (Ali et al., 2019; Arnell and Gosling,  
422 2016; Dottori et al., 2018; Hirabayashi et al., 2013; Milly et al., 2002). Thus, an effort is  
423 required to better understand flood generation mechanisms in the large river basins of the  
424 Indian Subcontinent during the monsoonal climate for effective flood management. In  
425 this study, we examined the temporal and spatial variability of hydrometeorological  
426 variables to identify the dominant flood-generating mechanisms and flood-contributing  
427 areas using the observed and VIC-simulated hydrological variables-

428 In our analysis, we considered two hydrometeorological variables, precipitation  
429 and surface runoff, across the basin to evaluate the flood generation mechanism where  
430 high-intensity precipitation is the primary driver in the flood occurrence. However,  
431 previous studies (Garg and Mishra, 2019; Sharma et al., 2018) showed that high-intensity



432 precipitation and floods are not always linked due to pre-hydrological conditions over the  
433 catchment. There is only 50 to 70% of high-intensity precipitation, which causes flooding  
434 in a basin (Garg and Mishra, 2019; Wasko and Sharma, 2017). Our results show that the  
435 attribution of high-intensity precipitation to flood generation varies with time. For  
436 instance, the majority of high-intensity precipitation events in the late monsoon season  
437 (August-September) cause flooding in the Godavari basin (Figure S3) due to wetter soil  
438 moisture conditions. Therefore, we used a bottom-up approach in our study to examine  
439 the temporal and spatial variability of hydrometeorological variables, i.e., we first  
440 identified the flood events, and then precipitation and surface runoff variables before the  
441 flood events were evaluated to understand their role in the flooding mechanism.

442 We evaluated the temporal properties of hydrometeorological variables  
443 (precipitation and surface runoff) to identify the flood types and processes (Keller et al.,  
444 2018; Merz and Blöschl, 2003) that predominantly occur over the Godavari basin in the  
445 monsoonal climate. We found that the majority of floods in the Godavari basin (except  
446 Mancherial Basin) are long-rain type floods (Keller et al., 2018; Merz and Blöschl,  
447 2003), which are associated with the 10 to 11 (7 to 8) days long precipitation (surface  
448 runoff) with multiple high-intensity precipitation events. However, the majority of floods  
449 in the semi-arid Mancherial sub-basin are short-rain type. The majority area of the  
450 Godavari basin, associated with long-duration precipitation (surface runoff), falls in the  
451 semi-humid climate. The rivers in the humid climate can carry a large volume of water  
452 (or have a large storage capacity); therefore, a significant amount of rainfall is required  
453 for the flood occurrence (Merz and Blöschl, 2003). Previous studies (Hirschboeck et al.,  
454 2000; Merz and Blöschl, 2003) have found that persistent rainfall in the region is the



455 primary factor in generating long-rain type floods. Consistent with our results, Merz and  
456 Blöschl, (2003) showed the long-rain type flood for most humid regions of Austria.  
457 Similarly, short-rain type flood in the semi-arid Mancherial region is associated with the  
458 small storage capacity of the river in the region, which can be easily achieved with  
459 shorter rainfall. Therefore, to minimize the risk of flooding in the region, we require a  
460 forecast system, which can predict the rainfall for 10 to 11 days duration in the semi-  
461 humid climate region. Moreover, we need to understand the occurrence of multiple  
462 concurrent extreme precipitation events in the future changing climate.

463 While the temporal properties of hydrometeorological variables have been widely  
464 evaluated to identify flood processes (Keller et al., 2018; Merz and Blöschl, 2003), the  
465 spatial patterns of hydrometeorology and catchment conditions before peak streamflow  
466 are commonly ignored. This study also evaluated the spatial variability of precipitation  
467 and surface runoff before peak streamflow to delineate the dominating flood-generating  
468 areas using the EOF and correlation analyses. We showed that the (long or short duration  
469 accumulated) precipitation and surface runoff before peak streamflow dominantly occur  
470 over the central and downstream areas of the Godavari basin, which contribute to the  
471 flood generation. Nied et al., (2014) found that the pre-event spatial patterns of  
472 hydrometeorological variables are linked with leading moisture transport and weather  
473 system patterns in the region. Moreover, the pre-event hydrometeorological patterns are  
474 also associated with the soil moisture patterns (Nied el al., 2014). Since the majority of  
475 floods in monsoonal climate occur during the wetter soil moisture condition, the soil  
476 moisture patterns may not affect the pre-event hydrometeorological patterns.



477 Apart from spatial patterns of precipitation and surface runoff prior to the flood,  
478 catchment properties also play an essential role in flood generation. We found that the  
479 majority area of the Tekra sub-basin generates more runoff compared to the other sub-  
480 basins. The high runoff ratio in the Tekra sub-basin can be associated with various  
481 catchment characteristics (such as high slope, forest-crop land cover, clay soil, etc.) in  
482 this semi-humid region, which results in a large fraction of precipitation contributing to  
483 the surface runoff and causing flooding in the downstream areas. Previous studies  
484 (Boardman et al., 2003; Holman et al., 2003; Lane, 2017; Marc and Robinson, 2007)  
485 showed that the high irrigation area, deforestation, and high slope accelerate the runoff  
486 generation mechanism, which causes high runoff in the basin.

487 With a limited understanding of flood processes in the Indian Subcontinent during the  
488 monsoonal climate, this study initiates a new discussion to better comprehend the flood  
489 generation mechanisms in India, aiming to improve flood management. Using the same  
490 approach, we can identify the temporal and spatial variability of hydrometeorological  
491 variables for the other Indian River basins, which can be used for numerous flood control  
492 applications. Overall, our findings provide a better insight into the flood generation  
493 mechanism over a large river basin of the Indian Subcontinent during the monsoonal  
494 climate. Based on our study, we conclude the following:

495 1. The majority of floods in the Godavari river basin occurred during the monsoon  
496 season. However, during the late monsoon, there is a higher ratio of high flood  
497 events to high precipitation events due to wet soil-moisture conditions.

498 2. Four out of five sub-basins (except the Mancherial sub-basin) showed the  
499 dominance of long-duration type floods in the period 1967-2019. Long-duration



500 (10-11 days) rainfall causes floods in the semi-humid region of Tekra,  
501 Pathagudam, Perur, and Polavaram sub-basins. However, Floods in the semi-arid  
502 Mancherial sub-basin are associated with short-duration (2 days) precipitation and  
503 surface runoff.

504 3. Floods in the Tekra, Pathagudam, Perur, and Polavaram sub-basins predominantly  
505 occur due to multiple high-intensity rainfall days. Therefore, long-duration type  
506 floods occurred in these sub-basins. Moreover, our analysis revealed that short-  
507 duration floods in the semi-arid Mancherial sub-basin are primarily associated  
508 with single-day high-intensity precipitation.

509 4. Based on the EOF and correlation analyses of precipitation and surface runoff,  
510 central and downstream areas of the basin dominate in the flood generation  
511 mechanism in the Godavari River, which highlights the importance of these areas  
512 in flood management in a future warming climate. Moreover, medium-term (10 to  
513 11 days lead) precipitation forecasts in these regions will be useful for flood and  
514 reservoir management forecasting.

515 5. Our analysis also indicated the importance of the Tekra sub-basin in the high  
516 runoff generation in the Godavari basin. Due to favorable catchment  
517 characteristics, a large fraction of precipitation contributes to the surface runoff in  
518 the Tekra sub-basin. Therefore, more efforts (i.e., afforestation and sustainable  
519 infrastructure development) are needed in the Tekra sub-basin for flood  
520 management in the downstream region.

521 In the changing climate and land use land cover (urbanization and deforestation), the  
522 risk of floods is projected to increase over the Indian Subcontinent (Ali et al., 2019;



523 Gosain et al., 2006; Gupta and Nair, 2011; Rogger et al., 2017; Shah et al., 2019).  
524 Moreover, the moisture-holding capacity of the atmosphere increases (Karl and  
525 Trenberth, 2003; Kharin et al., 2007) due to a warming climate, which leads to frequent,  
526 intense, and more extended extreme precipitation events (Ali et al., 2019, 2014; Roxy et  
527 al., 2017; Vittal et al., 2013). Therefore, reliable information on precipitation and runoff  
528 forecasts in the basin is crucial for effective flood mitigation. Moreover, significant steps  
529 are needed to reduce the rapid runoff generation in the Tekra sub-basin using natural  
530 flood management methods for flood control in the downstream area of the basin (Lane,  
531 2017). For instance, attenuation of surface runoff can be achieved through afforestation  
532 (Marc and Robinson, 2007), changes in arable land-use practices (Boardman et al., 2003),  
533 reductions in livestock density (Orr and Carling, 2006), and Changes in tillage practices  
534 (Holman et al., 2003). Along with the study of natural drivers of floods, we also have to  
535 analyze the role of human activities (intensive agriculture practices, reservoir operation,  
536 groundwater depletion, urbanization, etc.) in the occurrence of flood events in the future.

537 **6. Acknowledgements:**

538 The first author appreciates the funding support from Anusadhan National Research  
539 Foundation (ANRF) under the Startup Research Grant (SRG). The authors acknowledge  
540 the data availability from the India Meteorological Department (IMD), National Centers  
541 for Environmental Prediction- National Center for Atmospheric Research (NCEP-  
542 NCAR), and the Central Water Commission (CWC). The authors also acknowledge Mr.  
543 Shailesh Garg and Dr. Vimal Mishra for providing the calibrated soil parameter datasets  
544 for the Godavari River.

545 **7. Author contributions:**



546 SA and EM designed the study and wrote the manuscript. SA simulated the VIC model  
547 and performed the analysis. UG prepared the figures and partially contributed to the  
548 analysis.

549 **8. Competing interests:**

550 Authors declare no competing interests.

551 **9. Data Availability:**

552 All the datasets used in this study can be obtained from the corresponding author.

553 **10. Code Availability:**

554 Data processing scripts can be obtained from the corresponding author.

555 **11. References:**

556 Ali, H., Mishra, V., Pai, D.S., 2014. Observed and projected urban extreme rainfall  
557 events in India. *J. Geophys. Res. Atmos.* 119, 12,621-12,641.

558 <https://doi.org/10.1002/2014JD022264>

559 Ali, H., Modi, P., Mishra, V., 2019. Increased flood risk in Indian sub-continent under the  
560 warming climate. *Weather Clim. Extrem.* 25, 100212.

561 <https://doi.org/10.1016/j.wace.2019.100212>

562 Allan, R.P., Soden, B.J., 2007. Large discrepancy between observed and simulated  
563 precipitation trends in the ascending and descending branches of the tropical  
564 circulation. *Geophys. Res. Lett.* 34, L18705. <https://doi.org/10.1029/2007GL031460>

565 Arnell, N.W., Gosling, S.N., 2016. The impacts of climate change on river flood risk at



566 the global scale. *Clim. Change* 134, 387–401. <https://doi.org/10.1007/s10584-014-1084-5>

568 Berghuijs, W.R., Woods, R.A., Hutton, C.J., Sivapalan, M., 2016. Dominant flood  
569 generating mechanisms across the United States. *Geophys. Res. Lett.* 43, 4382–  
570 4390. <https://doi.org/10.1002/2016GL068070>

571 Blöschl, G., Hall, J., Parajka, J., Perdigão, R.A.P., Merz, B., Arheimer, B., Aronica, G.T.,  
572 Bilibashi, A., Bonacci, O., Borga, M., Ivan, Č., Castellarin, A., Chirico, G.B., 2017.  
573 European floods. *Science* (80-. ). 357, 588–590.  
574 <https://doi.org/10.1126/science.aan2506>

575 Blöschl, G., Nester, T., Komma, J., Parajka, J., Perdigão, R.A.P., 2013. The June 2013  
576 flood in the Upper Danube Basin, and comparisons with the 2002, 1954 and 1899  
577 floods. *Hydrol. Earth Syst. Sci.* 17, 5197–5212. <https://doi.org/10.5194/HESS-17-5197-2013>

579 Boardman, J., Evans, R., Ford, J., 2003. Muddy floods on the South Downs, southern  
580 England: problem and responses. *Environ. Sci. Policy* 6, 69–83.  
581 [https://doi.org/10.1016/S1462-9011\(02\)00125-9](https://doi.org/10.1016/S1462-9011(02)00125-9)

582 Brunner, M.I., Gilleland, E., Wood, A., Swain, D.L., Clark, M., 2020a. Spatial  
583 Dependence of Floods Shaped by Spatiotemporal Variations in Meteorological and  
584 Land-Surface Processes. *Geophys. Res. Lett.* 47, e2020GL088000.  
585 <https://doi.org/10.1029/2020GL088000>

586 Brunner, M.I., Papalexiou, S., Clark, M.P., Gilleland, E., 2020b. How Probable Is  
587 Widespread Flooding in the United States? *Water Resour. Res.* 56,



588 e2020WR028096. <https://doi.org/10.1029/2020WR028096>

589 Chawla, I., Mujumdar, P.P., 2015. Isolating the impacts of land use and climate change  
590 on streamflow. *Hydrol. Earth Syst. Sci.* 19, 3633–3651.  
591 <https://doi.org/10.5194/HESS-19-3633-2015>

592 Cherkauer, K.A., Bowling, L.C., Lettenmaier, D.P., 2003. Variable infiltration capacity  
593 cold land process model updates. *Glob. Planet. Change* 38, 151–159.  
594 [https://doi.org/10.1016/S0921-8181\(03\)00025-0](https://doi.org/10.1016/S0921-8181(03)00025-0)

595 Cherkauer, K.A., Lettenmaier, D.P., 1999. Hydrologic effects of frozen soils in the upper  
596 Mississippi River basin. *J. Geophys. Res. Atmos.* 104, 19599–19610.  
597 <https://doi.org/10.1029/1999JD900337>

598 Diederens, D., Liu, Y., Gouldby, B., Diermanse, F., Vorogushyn, S., 2019. Stochastic  
599 generation of spatially coherent river discharge peaks for continental event-based  
600 flood risk assessment. *Nat. Hazards Earth Syst. Sci.* 19, 1041–1053.  
601 <https://doi.org/10.5194/NHESS-19-1041-2019>

602 Dottori, F., Szewczyk, W., Ciscar, J.-C., Zhao, F., Alfieri, L., Hirabayashi, Y., Bianchi,  
603 A., Mongelli, I., Frieler, K., Betts, R.A., Feyen, L., 2018. Increased human and  
604 economic losses from river flooding with anthropogenic warming. *Nat. Clim.  
605 Chang.* 8, 781–786. <https://doi.org/10.1038/s41558-018-0257-z>

606 Fischer, G., Nachtergaele, F., Prieler, S., Velthuizen, H.T. van, Verelst, L., Wiberg, D.,  
607 2008. Global Agro-ecological Zones Assessment for Agriculture [WWW  
608 Document]. IIASA, Laxenburg, Austria FAO, Rome, Italy. URL  
609 <https://www.fao.org/soils-portal/data-hub/soil-maps-and-databases/harmonized->



610 world-soil-database-v12/en/

611 Gao, H., Birkett, C., Lettenmaier, D.P., 2012. Global monitoring of large reservoir  
612 storage from satellite remote sensing. *Water Resour. Res.* 48.

613 <https://doi.org/10.1029/2012WR012063>

614 Gao, H., Tang, Q., Shi, X., Zhu, C., Bohn, T.J., Su, F., Sheffield, J., Pan, M.,  
615 Lettenmaier, D.P., Wood, E.F., 2010. Water budget record from Variable Infiltration  
616 Capacity (VIC) model. *Algorithm Theor. Basis Doc. Terr. Water Cycle Data Rec.*

617 Garg, S., Mishra, V., 2019. Role of Extreme Precipitation and Initial Hydrologic  
618 Conditions on Floods in Godavari River Basin, India. *Water Resour. Res.* 55, 9191–  
619 [9210. https://doi.org/10.1029/2019WR025863](https://doi.org/10.1029/2019WR025863)

620 Gosain, A.K., Rao, S., Basuray, D., 2006. Climate change impact assessment on  
621 hydrology of Indian river basins. *Curr. Sci.* 90, 346–353.

622 Grams, C.M., Binder, H., Pfahl, S., Piaget, N., Wernli, H., 2014. Atmospheric processes  
623 triggering the central European floods in June 2013. *Nat. Hazards Earth Syst. Sci.*  
624 14, 1691–1702. <https://doi.org/10.5194/NHESS-14-1691-2014>

625 Guerreiro, S.B., Fowler, H.J., Barbero, R., Westra, S., Lenderink, G., Blenkinsop, S.,  
626 Lewis, E., Li, X.-F., 2018. Detection of continental-scale intensification of hourly  
627 rainfall extremes. *Nat. Clim. Chang.* 8, 803–807. <https://doi.org/10.1038/s41558-018-0245-3>

629 Gupta, A.K., Nair, S.S., 2011. Urban floods in Bangalore and Chennai: risk management  
630 challenges and lessons for sustainable urban ecology. *Curr. Sci.* 100, 1638–1645.



631 Hansen, M.C., DeFries, R.S., Townshend, J.R., Sohlberg, R., 2000. Global land cover  
632 classification at 1 km spatial resolution using a classification tree approach. *Int. J.*  
633 *Remote Sens.* 21, 1331–1364.

634 Hirabayashi, Y., Mahendran, R., Koitala, S., Konoshima, L., Yamazaki, D., Watanabe,  
635 S., Kim, H., Kanae, S., 2013. Global flood risk under climate change. *Nat. Clim.*  
636 *Chang.* 3, 816–821. <https://doi.org/10.1038/nclimate1911>

637 Hirschboeck, K.K., Ely, L., Maddox, R.A., 2000. Hydroclimatology of meteorologic  
638 floods, in: Wohl, E. (Ed.), *In Inland Flood Hazards: Human, Riparian and*  
639 *Aquatic Communities*. Cambridge University Press, New York, pp. 39–72.

640 Holman, I.P., Hollis, J.M., Bramley, M.E., Thompson, T.R.E., 2003. The contribution of  
641 soil structural degradation to catchment flooding: a preliminary investigation of the  
642 2000 floods in England and Wales. *Hydrol. Earth Syst. Sci.* 7, 755–766.  
643 <https://doi.org/10.5194/HESS-7-755-2003>

644 Karl, T.R., Trenberth, K.E., 2003. Modern global climate change. *Science* 302, 1719–23.  
645 <https://doi.org/10.1126/science.1090228>

646 Keller, L., Rössler, O., Martius, O., Weingartner, R., 2018. Delineation of flood  
647 generating processes and their hydrological response. *Hydrol. Process.* 32, 228–240.  
648 <https://doi.org/10.1002/HYP.11407>

649 Kharin, V. V., Zwiers, F.W., Zhang, X., Hegerl, G.C., 2007. Changes in temperature and  
650 precipitation extremes in the IPCC ensemble of global coupled model simulations. *J.*  
651 *Clim.* 20, 1419–1444.



652 Kundzewicz, Z.W., Kanae, S., Seneviratne, S.I., Handmer, J., Nicholls, N., Peduzzi, P.,  
653 Mechler, R., Bouwer, L.M., Arnell, N., Mach, K., Muir-Wood, R., Brakenridge,  
654 G.R., Kron, W., Benito, G., Honda, Y., Takahashi, K., Sherstyukov, B., 2014. Flood  
655 risk and climate change: global and regional perspectives. *Hydrol. Sci. J.* 59, 1–28.  
656 <https://doi.org/10.1080/02626667.2013.857411>

657 Lane, S.N., 2017. Natural flood management. *WIREs Water* 4.  
658 <https://doi.org/10.1002/WAT2.1211>

659 Li, D., Lettenmaier, D.P., Margulis, S.A., Andreadis, K., 2019. The Role of Rain-on-  
660 Snow in Flooding Over the Conterminous United States. *Water Resour. Res.* 55,  
661 8492–8513. <https://doi.org/10.1029/2019WR024950>

662 Liang, X., Lettenmaier, D.P., Wood, E.F., Burges, S.J., 1994. A simple hydrologically  
663 based model of land surface water and energy fluxes for general circulation models.  
664 *J. Geophys. Res. Atmos.* 99, 14415–14428.

665 Liang, X., Wood, E.F., Lettenmaier, D.P., 1996. Surface soil moisture parameterization  
666 of the VIC-2L model: Evaluation and modification. *Glob. Planet. Change* 13, 195–  
667 206.

668 Lindell, M.K., Arlikatti, S., Huang, S.K., 2019. Immediate behavioral response to the  
669 June 17, 2013 flash floods in Uttarakhand, North India. *Int. J. Disaster Risk Reduct.*  
670 34, 129–146. <https://doi.org/10.1016/J.IJDRR.2018.11.011>

671 Lohmann, D., NOLTE-HOLUBE, R., RASCHKE, E., 1996. A large-scale horizontal  
672 routing model to be coupled to land surface parametrization schemes. *Tellus A* 48,  
673 708–721. <https://doi.org/10.1034/j.1600-0870.1996.t01-3-00009.x>



674 Mahto, S.S., Mishra, V., 2019. Does ERA-5 Outperform Other Reanalysis Products for  
675 Hydrologic Applications in India? *J. Geophys. Res. Atmos.* 124, 9423–9441.  
676 <https://doi.org/10.1029/2019JD031155>

677 Marc, V., Robinson, M., 2007. The long-term water balance (1972-2004) of upland  
678 forestry and grassland at Plynlimon, mid-Wales. *Hydrol. Earth Syst. Sci.* 11, 44–60.  
679 <https://doi.org/10.5194/HESS-11-44-2007>

680 Maurer, E.P., Wood, A.W., Adam, J.C., Lettenmaier, D.P., 2002. A long-term  
681 hydrologically based dataset of land surface fluxes and states for the conterminous  
682 United States. *Am. Meteorol. Soc.* 21, 116–119. <https://doi.org/10.1175/JCLI-D-12-00508.1>

684 Merz, R., Blöschl, G., 2003. A process typology of regional floods. *Water Resour. Res.*  
685 39, 1340. <https://doi.org/10.1029/2002WR001952>

686 Milly, P.C.D., Wetherald, R.T., Dunne, K.A., Delworth, T.L., 2002. Increasing risk of  
687 great floods in a changing climate. *Nature* 415, 514–517.

688 Min, S.-K., Zhang, X., Zwiers, F.W., Hegerl, G.C., 2011. Human contribution to more-  
689 intense precipitation extremes. *Nature* 470. <https://doi.org/10.1038/nature09763>

690 Mishra, V., Aadhar, S., Shah, H., Kumar, R., Pattanaik, D.R., Tiwari, A.D., 2018. The  
691 Kerala flood of 2018: combined impact of extreme rainfall and reservoir storage.  
692 *Hydrol. Earth Syst. Sci. Discuss.* 1–13. <https://doi.org/10.5194/hess-2018-480>

693 Mishra, V., Smoliak, B. V., Lettenmaier, D.P., Wallace, J.M., 2012. A prominent pattern  
694 of year-to-year variability in Indian Summer Monsoon Rainfall. *Proc. Natl. Acad.*



695 Sci. 109, 7213–7217. <https://doi.org/10.1073/pnas.1119150109>

696 Mujumdar, G.G., Rajaguru S. N., Pappu R. S., 1969. THE RECENT GODAVARI  
697 FLOOD (SEPTEMBER 1969) AND ITS RELEVANCE TO PREHISTORIC  
698 ARCHAEOLOGY on JSTOR. Bull. Deccan Coll. Post-Graduate Res. Inst. 29, 118–  
699 134.

700 Nageswara Rao, G., 2001. Occurrence of heavy rainfall around the confluence line in  
701 monsoon disturbances and its importance in causing floods. Proc. Indian Acad. Sci.  
702 Earth Planet. Sci. 110, 87–94. <https://doi.org/10.1007/bf02702232>

703 Nanditha, J.S., Mishra, V., 2022. Multiday Precipitation Is a Prominent Driver of Floods  
704 in Indian River Basins. Water Resour. Res. 58, e2022WR032723.  
705 <https://doi.org/10.1029/2022WR032723>; REQUESTEDJOURNAL:JOURNAL:1944  
706 7973;WGROUP:STRING:PUBLICATION

707 Nanditha, J.S., Rajagopalan, B., Mishra, V., 2022. Combined signatures of atmospheric  
708 drivers, soil moisture, and moisture source on floods in Narmada River basin, India.  
709 Clim. Dyn. 2022 599 59, 2831–2851. <https://doi.org/10.1007/S00382-022-06244-X>

710 Nash, J.E., Sutcliffe, J.V., 1970. River flow forecasting through conceptual models part I  
711 — A discussion of principles. J. Hydrol. 10, 282–290. [1694\(70\)90255-6](https://doi.org/10.1016/0022-<br/>712 1694(70)90255-6)

713 Nied, M., Pardowitz, T., Nissen, K., Ulbrich, U., Hundecha, Y., Merz, B., 2014. On the  
714 relationship between hydro-meteorological patterns and flood types. J. Hydrol. 519,  
715 3249–3262. <https://doi.org/10.1016/J.JHYDROL.2014.09.089>



716 Orr, H.G., Carling, P.A., 2006. Hydro-climatic and land use changes in the River Lune  
717 catchment, North West England, implications for catchment management. *River*  
718 *Res. Appl.* 22, 239–255. <https://doi.org/10.1002/RRA.908>

719 Pai, D.S., Sridhar, L., Badwaik, M.R., Rajeevan, M., 2015. Analysis of the daily rainfall  
720 events over India using a new long period (1901–2010) high resolution ( $0.25^\circ \times$   
721  $0.25^\circ$ ) gridded rainfall data set. *Clim. Dyn.* 45, 755–776.  
722 <https://doi.org/10.1007/s00382-014-2307-1>

723 Pai, D.S., Sridhar, L., Rajeevan, M., Sreejith, O.P., Satbhai, N.S., Mukhopadhyay, B.,  
724 2014. Development of a new high spatial resolution ( $0.25^\circ \times 0.25^\circ$ ) long period  
725 (1901–2010) daily gridded rainfall data set over India and its comparison with  
726 existing data sets over the region. *Mausam* 65, 1–18.

727 Rajeevan, M., Unnikrishnan, C.K., Preethi, B., 2012. Evaluation of the ENSEMBLES  
728 multi-model seasonal forecasts of Indian summer monsoon variability. *Clim. Dyn.*  
729 38, 2257–2274. <https://doi.org/10.1007/s00382-011-1061-x>

730 Rakhecha, P., Singh, V., 2017. Enveloping Curves for the Highest Floods of River basins  
731 in India. *Int. J. Hydrol.* 1. <https://doi.org/10.15406/ijh.2017.01.00015>

732 Rakhecha, P.R., 2002. Highest floods in India. *IAHS Publ.* 167–172.

733 Ray, K., Pandey, P., Pandey, C., Dimri, A.P., Kishore, K., 2019. On the recent floods in  
734 India. *Curr. Sci.* 117, 204–218.

735 Ren-Jun, Z., 1992. The Xinanjiang model applied in China. *J. Hydrol.* 135, 371–381.  
736 [https://doi.org/10.1016/0022-1694\(92\)90096-E](https://doi.org/10.1016/0022-1694(92)90096-E)



737 Rogger, M., Agnoletti, M., Alaoui, A., Bathurst, J.C., Bodner, G., Borga, M., Chaplot,  
738 V., Gallart, F., Glatzel, G., Hall, J., Holden, J., Holko, L., Horn, R., Kiss, A.,  
739 Kohnová, S., Leitinger, G., Lennartz, B., Parajka, J., Perdigão, R., Peth, S.,  
740 Plavcová, L., Quinton, J.N., Robinson, M., Salinas, J.L., Santoro, A., Szolgay, J.,  
741 Tron, S., Akker, J.J.H. van den, Viglione, A., Blöschl, G., 2017. Land use change  
742 impacts on floods at the catchment scale: Challenges and opportunities for future  
743 research. *Water Resour. Res.* 53, 5209–5219.  
744 <https://doi.org/10.1002/2017WR020723>

745 Roxy, M.K., Ghosh, S., Pathak, A., Athulya, R., Mujumdar, M., Murtugudde, R., Terray,  
746 P., Rajeevan, M., 2017. A threefold rise in widespread extreme rain events over  
747 central India. *Nat. Commun.* 8. <https://doi.org/10.1038/s41467-017-00744-9>

748 Shah, H.L., Mishra, V., 2016. Hydrologic changes in Indian subcontinental river basins  
749 (1901–2012). *J. Hydrometeorol.* 17, 2667–2687. <https://doi.org/10.1175/JHM-D-15-0231.1>

751 Shah, H.L., Zhou, T., Sun, N., Huang, M., Mishra, V., 2019. Roles of Irrigation and  
752 Reservoir Operations in Modulating Terrestrial Water and Energy Budgets in the  
753 Indian Subcontinental River Basins. *J. Geophys. Res. Atmos.* 124, 12915–12936.  
754 <https://doi.org/10.1029/2019JD031059>

755 Sharma, A., Wasko, C., Lettenmaier, D.P., 2018. If Precipitation Extremes Are  
756 Increasing, Why Aren't Floods? *Water Resour. Res.* 54, 8545–8551.  
757 <https://doi.org/10.1029/2018WR023749>

758 Sheffield, J., Wood, E.F., 2007. Characteristics of global and regional drought, 1950–



759 2000: Analysis of soil moisture data from off-line simulation of the terrestrial  
760 hydrologic cycle. *J. Geophys. Res.* 112, D17115.  
761 <https://doi.org/10.1029/2006JD008288>

762 Sikorska, A.E., Vivenioli, D., Seibert, J., 2015. Flood-type classification in mountainous  
763 catchments using crisp and fuzzy decision trees. *Water Resour. Res.* 51, 7959–7976.  
764 <https://doi.org/10.1002/2015WR017326>

765 Srivastava, A.K., Rajeevan, M., Kshirsagar, S.R., 2009. Development of a high resolution  
766 daily gridded temperature data set (1969-2005) for the Indian region. *Atmos. Sci.  
767 Lett.* 10, 249–254. <https://doi.org/10.1002/asl.232>

768 Tarasova, L., Merz, R., Kiss, A., Basso, S., Blöschl, G., Merz, B., Viglione, A., Plötner,  
769 S., Guse, B., Schumann, A., Fischer, S., Ahrens, B., Anwar, F., Bárdossy, A.,  
770 Bühler, P., Haberlandt, U., Kreibich, H., Krug, A., Lun, D., Müller-Thomy, H.,  
771 Pidoto, R., Primo, C., Seidel, J., Vorogushyn, S., Wietzke, L., 2019. Causative  
772 classification of river flood events. *Wiley Interdiscip. Rev. Water* 6, e1353.  
773 <https://doi.org/10.1002/WAT2.1353>

774 The Hindu, 2011. When Bhadrachalam was under a sheet of water. *The Hindu*.

775 Trenberth, K.E., Dai, A., Rasmussen, R.M., Parsons, D.B., 2003. The Changing  
776 Character of Precipitation. *Bull. Am. Meteorol. Soc.* 84, 1205–1218.  
777 <https://doi.org/10.1175/BAMS-84-9-1205>

778 Ummenhofer, C.C., Gupta, A. Sen, Li, Y., Taschetto, A.S., England, M.H., 2011. Multi-  
779 decadal modulation of the El Niño-Indian monsoon relationship by Indian Ocean  
780 variability. *Environ. Res. Lett* 6, 34006–34014. <https://doi.org/10.1088/1748->



781 9326/6/3/034006

782 Viglione, A., Chirico, G.B., Komma, J., Woods, R., Borga, M., Blöschl, G., 2010.

783 Quantifying space-time dynamics of flood event types. *J. Hydrol.* 394, 213–229.

784 <https://doi.org/10.1016/J.JHYDROL.2010.05.041>

785 Vittal, H., Karmakar, S., Ghosh, S., 2013. Diametric changes in trends and patterns of

786 extreme rainfall over India from pre-1950 to post-1950. *Geophys. Res. Lett.* 40,

787 3253–3258. <https://doi.org/10.1002/GRL.50631>

788 Wasko, C., Sharma, A., 2017. Global assessment of flood and storm extremes with

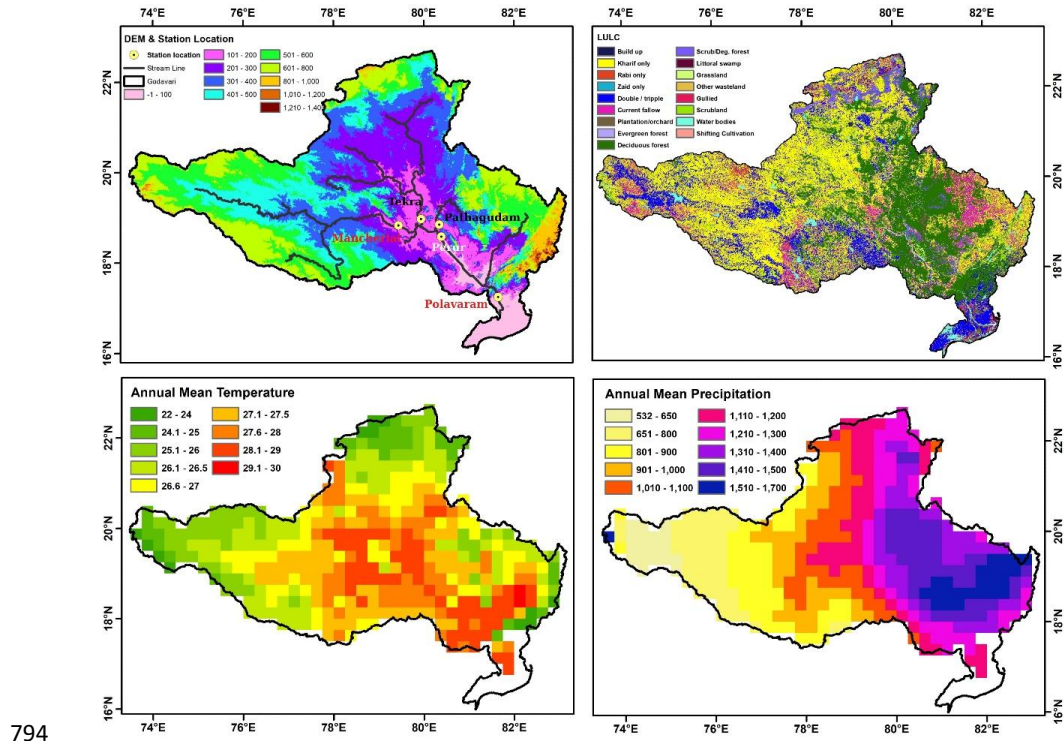
789 increased temperatures. *Sci. Reports* 2017 71 7, 1–8. [https://doi.org/10.1038/s41598-](https://doi.org/10.1038/s41598-017-08481-1)

790 017-08481-1

791

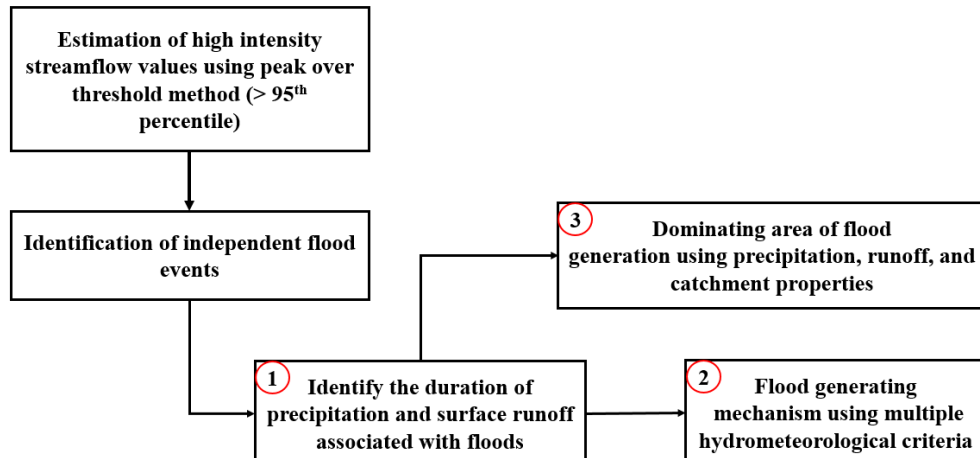
792

793 **12. Figures & Tables:**



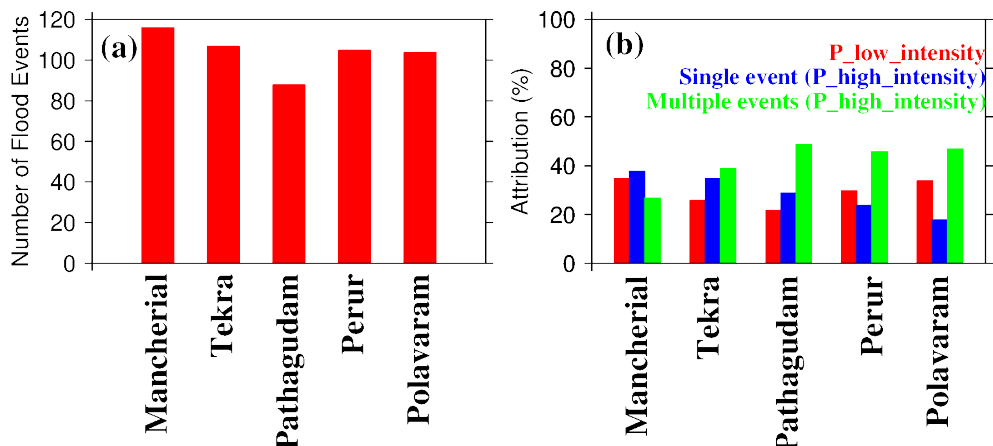
794

795 **Figure 1: Catchment and climate information of Godavari river.** (a-b) Topographic  
796 using the Digital Elevation Map (DEM) and Land use land cover (LULC) information of  
797 the Godavari river basin. (c-d) Climate conditions over the basin using the annual mean  
798 temperature and precipitation during 1967-2019.



800 **Figure 2. Major steps used in the analysis.**

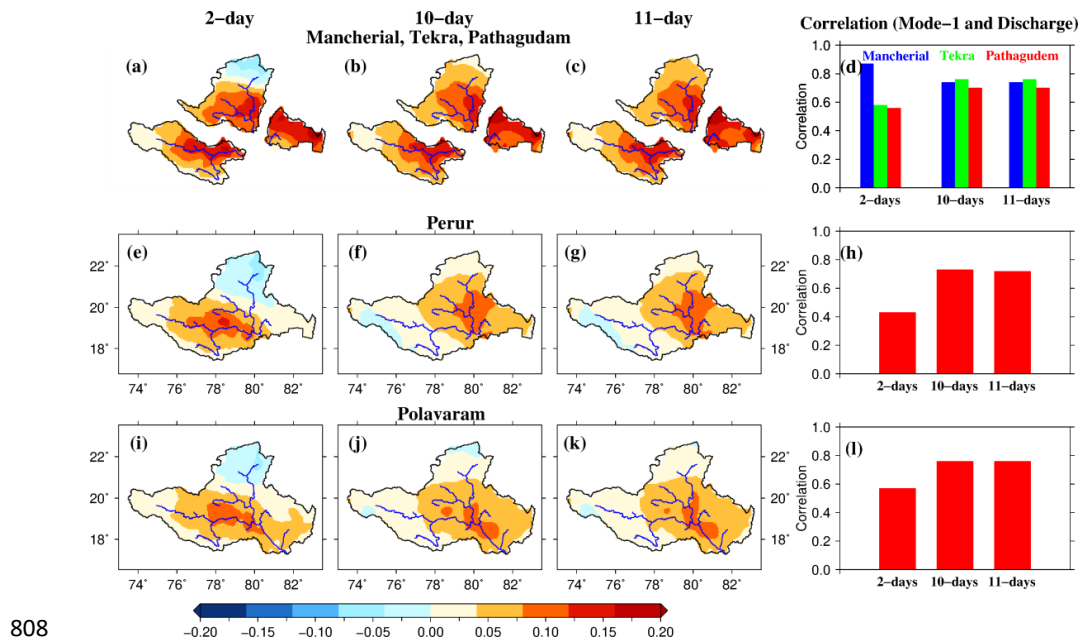
801



803 **Figure 3. Floods associated with multiple criteria of precipitation over Godavari**

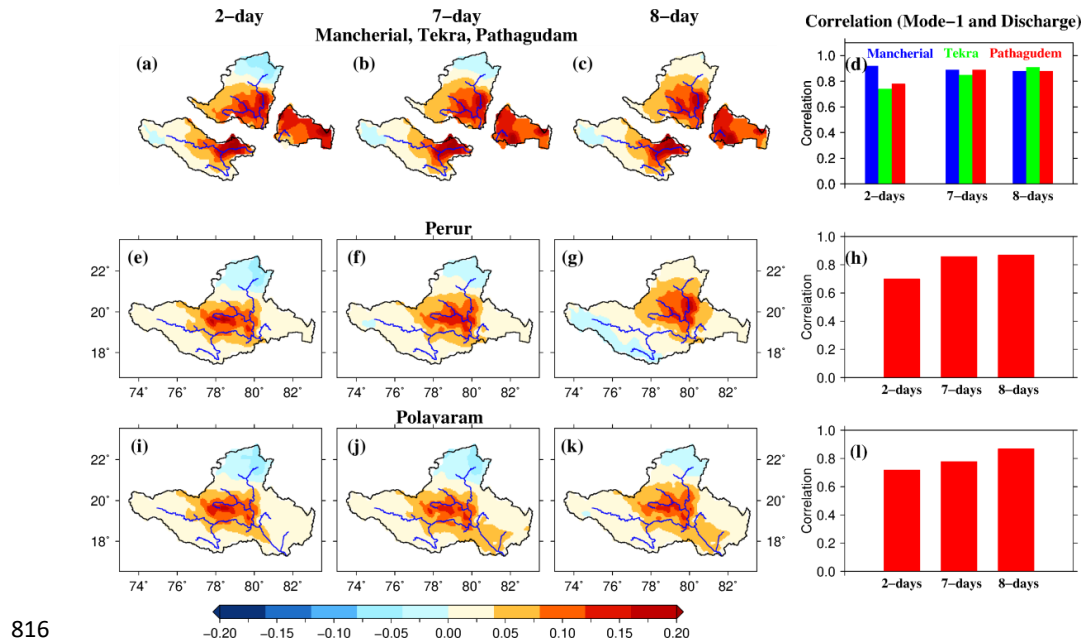
804 **River Basin.** (a) number of flood events in each sub-basin. (b) Attribution (%) of low-  
805 intensity precipitation, single high-intensity precipitation, and multiple days' high-  
806 intensity precipitation in flood generation.

807



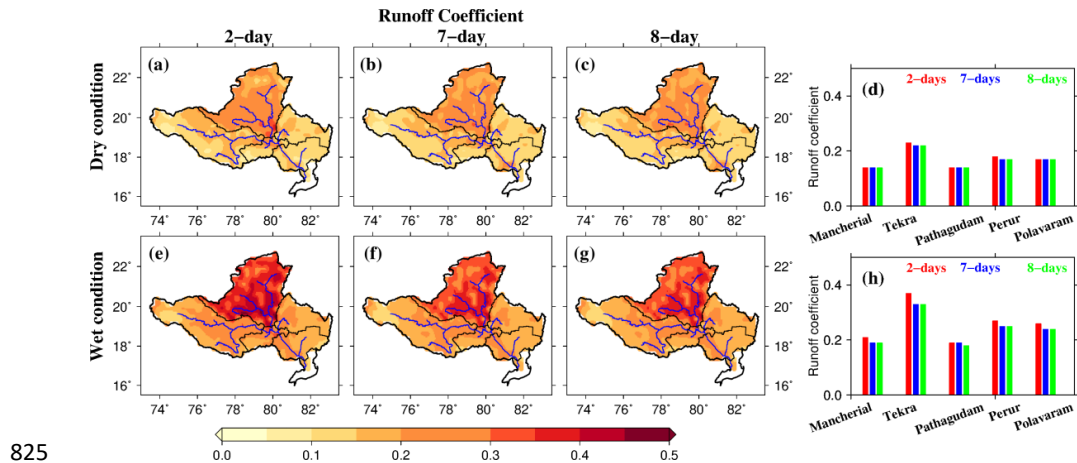
808 **Figure 4:** The leading mode of variability in the accumulated precipitation during the high  
809 streamflow events for the period 1967-2019 using the method of empirical orthogonal function  
810 (EOF). (a-c) The first leading EOF mode of (a) 2-days, (b) 10-days, and (c) 11-days accumulated  
811 precipitation for the Polavaram sub-basin. (d) Correlation between first leading mode and flood  
812 peak at the Polavaram station. (e-h) same as (a-d) but for Perur sub-basin. (i-l) same as (a-d) but  
813 for Mancherial (left), Tekra (middle), and Pathagudam (right) sub-basins.

814  
815



816  
817 **Figure 5.** The leading mode of variability in the accumulated runoff (excess precipitation) during  
818 the extreme floods for the period 1967-2019 using the method of empirical orthogonal function  
819 (EOF). (a-c) The first leading EOF mode of (a) 2-days, (b) 7-days, and (c) 8-days accumulated  
820 runoff for Polavaram sub-basin. (d) Correlation between first leading principle component (PC-1)  
821 and extreme floods over at Polavaram station during 1967-2019 for 2, 7, and 8-days accumulated  
822 runoff. (e-h) same as (a-d) but for Perur sub-basin. (i-l) same as (a-d) but for Mancherial (left),  
823 Tekra (middle), and Pathagudam (right) sub-basins.

824



825 **Figure 6.** Runoff coefficient over Godavari basin during the flood events in the period  
826 1967-2019. (a-c) Variability in runoff coefficient values using (a) 2-days, (b) 7-days, and  
827 (c) 8-days cumulative precipitation and runoff during dry condition flood events. (d-f)  
828 Similar to (a-c) but variability in runoff coefficient values during wet condition flood  
829 events.  
830

831

832

833 **Table 1:** Duration and lag (days) where the basin-averaged accumulated precipitation has  
834 the highest correlation with simulated flood peak for high streamflow events at different  
835 stations.

Station	Lag-time	Duration
Mancherial	2	2
Tekra	1	11
Pathagudam	2	10



Perur	2	10
Polavaram	2	11

836

837

838 **Table 2:** Duration and lag (days) where the basin-averaged simulated accumulated  
839 surface runoff has the highest correlation with the simulated flood peak for high  
840 streamflow events at different stations

Station	Lag-time	Duration
Mancherial	2	2
Tekra	1	8
Pathagudam	2	7
Perur	2	7
Polavaram	2	7

841